Pulsed Terahertz Attenuated Total Reflection Spectroscopy

DAVID A. NEWNHAM* and PHILIP F. TADAY†

TeraView Limited, Platinum Building, St John's Innovation Park, Cambridge, CB4 0WS, United Kingdom

Pulsed terahertz attenuated total reflection (ATR) spectra of solid materials and liquids covering the 10 cm^{-1} to 120 cm^{-1} (0.3 THz to 3.6 THz) region of the electromagnetic spectrum are recorded using a terahertz pulsed spectrometer and silicon ATR modules. Pulsed terahertz ATR measurements are completed nondestructively using small amounts of sample (typically 1 mg for solids) and no sample preparation. Many terahertz analyses can be run in rapid sequence, minimizing the analysis time.

Index Headings: **Terahertz; Attenuated total reflection; ATR; Far infrared.**

INTRODUCTION

Terahertz pulsed spectroscopy has made working in the far-infrared region straightforward. Between 1.2 cm^{-1} and 120 cm^{-1} corresponding to frequencies 36 GHz and 3.6 THz, low-frequency motions in molecular systems can be explored. These motions involve flexing of the individual molecules or intermolecular interactions via either strong hydrogen bonds or weaker van der Waals bonding between neighboring molecules. This allows polymorphs,[1–4] hydrates,[5,6] and solvates of solid crystalline[4,7] materials to be characterized, which is of great interest to the pharmaceutical industry. For high molecular weight species, including metallic complexes and biomolecules such as proteins, probing the intramolecular vibrations that occur in the far-infrared (FIR) region below 12 THz (400 cm^{-1}) provides insights into structural dynamics.

Traditionally radiation in the low-frequency part of the electromagnetic spectrum has been generated by sources of incoherent blackbody radiation such as mercury arc lamps. Cryogen-cooled bolometers were necessary to detect the signals. Due to the difficulties arising from the combination of weak sources of radiation and the elaborate detection process, only few specialist groups have been studying material properties in this spectral range. The measurements have been very time consuming and, in addition to the need for a constant supply of cryogens, the instruments are very difficult to maintain.

Terahertz photoconductive emitters generate terahertz pulses using an ultrafast (femtosecond) laser to excite a biased gallium arsenide antenna.[8] This technique is inherently broadband, with the emitted power distributed over a frequency range of several THz (typically 2 cm^{-1} to 120 cm^{-1}, corresponding to 0.06 THz to 3.6 THz). Pulsed terahertz emission in photoconductive antennae is produced when the current density, $\mathbf{j}$, of a biased semiconductor is modulated on subpicosecond timescales $\mathbf{E}_{THz} \propto d\mathbf{j}/dt$. The change in current density, and hence photocurrent, arises from two processes: (1) the rapid change of the carrier density via femtosecond laser illumination, and (2) the acceleration of photo-generated carriers under an external electric field.

Coherent detection of the terahertz radiation is performed in a similar photoconductive antenna circuit. By gating the photoconductive gap with a femtosecond pulse synchronized to the terahertz emission, a current proportional to the terahertz electric field is measured. By varying the optical path length to the receiver, the terahertz time domain signal can be sampled. Hence, both the amplitude and phase of the incident terahertz wave can be obtained and a source signal strengthening of >70 dB can be achieved using time-gated detection.[9] The technique has a very high signal-to-noise ratio over the spectral range 5 cm^{-1} to 100 cm^{-1}.

Terahertz pulsed instruments require little maintenance and are relatively compact and mobile as there is no need for sophisticated cooling solutions. The average power of the terahertz radiation used for the measurements is below 1 μW so no thermal strain is induced in the sample as this level of radiation is below the level of thermal background radiation. To date, most pulsed terahertz measurements have been completed in either a polyethylene matrix (see for example Refs. 1–5) or a PTFE matrix (for example, Ref. 10). This involves mixing and compressing the sample of interest, which could induce a polymorphic change in the sample. The sample is also difficult to recover from the procedure and relatively large amounts of samples are required (20–100 mg).

Single reflection attenuated total reflection (ATR) accessories greatly simplify the collection of spectra due to the ease and speed of sampling. The ATR technique uses a small sampling area, requires no sample preparation, is nondestructive, and changing samples does not interfere with the purge on the spectrometer. The ATR measurement is made simply by placing a small amount of powder or liquid sample onto the ATR crystal. For solids applying load achieves full contact with the ATR crystal and maximizes the absorbance. The sample does not need to be ground up or mixed with another material like polyethylene and can be collected afterwards. This differs from the previous reported terahertz ATR measurements where the sample was not in full contact with the crystal.[11] A single reflection approach was taken by Nagai et al.,[12] who used an electro-optic sampling (EOS) technique for the detection of the terahertz pulse. The EOS technique results in multiple reflections in the time-domain data due to reflections in the detection crystal. This results in possible interference with the acquired ATR spectrum. These multiple reflections are removed by using a photoconductive emitter which is out-coupled with a silicon lens and a GaAs photoconductive receiver as used in this paper.

The principle of the terahertz ATR technique is shown in Fig. 1. The terahertz pulsed beam is brought to a focus at the horizontal ATR crystal surface using a z-cut quartz condensing lens. The ATR crystal material is chosen to have suitable optical and mechanical properties. Silicon crystals are hard wearing, resistant to chemical attack, isotropic, and have low

Received 11 September 2007; accepted 10 January 2008.

* Current address: Qi3, St. John's Innovation Centre, Cowley Road, Cambridge, CB4 0WS, United Kingdom.

† Author to whom correspondence should be sent. E-mail: philip.taday@teraview.com.

0003-7028/08/6204-0394$2.00/0

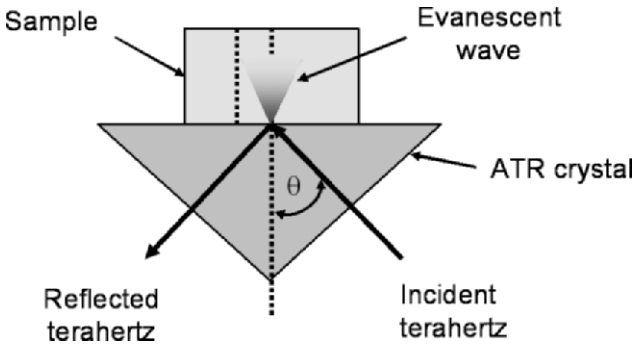

FIG. 1. Schematic illustration of the terahertz ATR sampling technique.

dispersion and transmission losses with a terahertz refractive index of 3.42. Germanium, with a terahertz refractive index of 4, would be another suitable ATR material. The silicon ATR crystals are cut at an angle of either 35° or 45°. The incident *p*-polarized terahertz beam makes incident cone angles of 0° and 10° with the surface normal of the entry face of the respective crystal due to the *f*/2 optics used. The beam is refracted from a central angle, θ, which equals either 45° or 38° onto the horizontal sampling interface with a wavenumber-dependent variation of up to ±5°. The terahertz beam is reflected at the sampling interface. When a sample is present an evanescent wave penetrates into the sample material to a penetration depth that depends on wavenumber, the refractive index of the sample and ATR crystal, the angle of incidence of the beam, and polarization. Penetration depth is defined as the depth at which the intensity of electromagnetic radiation penetrating into material or an object falls to 1/*e* of the original value at the surface. The penetration depth is effectively given by 1/α, where α is the absorption coefficient or molar absorptivity of a material. It is related to the Beer–Lambert law, were the strength of the electromagnetic wave inside the material $E^2(z) = E_0^2 e^{-\alpha z}$ (where E_0 is the electric field strength of radiation incident at the surface and z is depth into the material). The effective thickness of the electric field propagating into the material is polarization dependent[13] and is given by

$$d_{e\perp} = [n_1^2 n_2 \cos\theta/(n_1^2 - n_2^2)]\lambda/\left(\pi\sqrt{n_1^2 \sin^2\theta - n_2^2}\right) \quad (1)$$

and

$$d_{e\|} = [n_1^2 n_2 \cos\theta/(n_1^2 - n_2^2)] \times \{(2n_1^2 \sin^2\theta - n_2^2)/[(n_1^2 + n_2^2)\sin^2\theta - n_2^2]\}\lambda \div \left(\pi\sqrt{n_1^2 \sin^2\theta - n_2^2}\right) \quad (2)$$

where n_1 is the refractive index of the ATR crystal, n_2 is the refractive index of the media under investigation, λ is the wavelength, and θ is the angle of the incident beam on the ATR crystal surface. For the parallel *p*-polarized beam the penetration depth is approximately double that with the perpendicularly *s*-polarized radiation. For the terahertz region the calculated penetration depths with parallel *p*-polarization, plotted in Fig. 2, are greater than in the mid-infrared region. As there is a wavenumber-dependent variation in penetration depth, the ATR signal must be corrected to approximately the

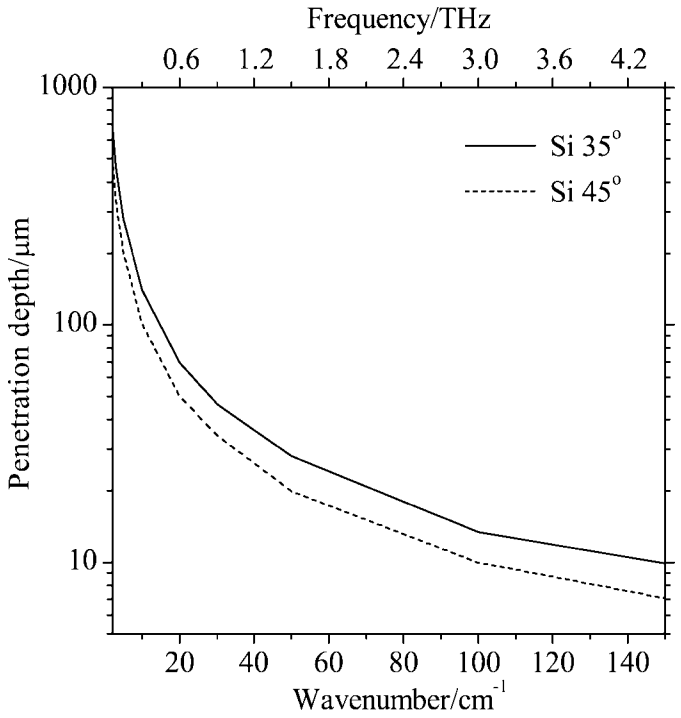

FIG. 2. Calculated wavenumber-dependent variation of terahertz penetration depth into sample with refractive index of 1.3, for silicon 35° and 45° crystals and parallel *p*-polarization.

correct absorption by the relationship

$$A(\tilde{\nu}) = \text{ATRsignal}(\tilde{\nu})/\tilde{\nu}_c \quad (3)$$

where $\tilde{\nu}_c$ is the center wavenumber for normalizing the absorbance. However, care should be taken with materials with a high absorption, such as water, as Eqs. 1 and 2 are broken. This is due the propagation length of the evanescent wave being comparable with the attenuation length in media; a more detailed analysis is given by Ekgasit in Ref. 14, who showed in this paper that the reflected ATR signal is not proportional to the absorption coefficient in strongly absorbing media. This will be explored in future work in the terahertz region where the propagation depths can be much greater than in the traditional mid-infrared region.

To optimize absorption by the sample for high concentration and low concentration components, ATR modules with different crystal angle and material can be used.

In this work the performance of a terahertz pulsed spectrometer and silicon ATR modules is presented.

EXPERIMENTAL

Attenuated total reflection spectra were collected from 10 cm^{-1} to 120 cm^{-1} (0.3 THz to 3.6 THz) at 1.2 cm^{-1} (0.04 THz) resolution using a TPS spectra 2000 terahertz pulsed spectrometer (TeraView, Cambridge, UK) with 35° and 45° silicon ATR modules. To remove spectral contributions associated with atmospheric moisture the system was purged with dry nitrogen (10 L/min). Solid sample spectra were referenced against a poly(tetrafluoroethylene) disk; for liquids the reference was the clean ATR crystal. For each rapid-scan measurement the average of 1800 scans was recorded in one minute and Blackman–Harris apodization was applied.

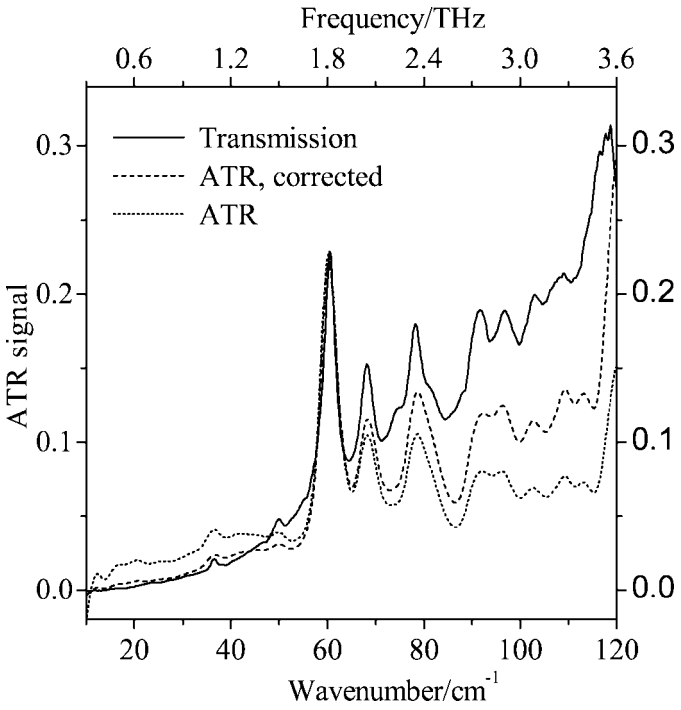

FIG. 3. Terahertz ATR measurements of L-ascorbic acid showing ATR signal and absorbance spectrum, corrected for penetration depth. Transmission measurement is shown for comparison.

One milligram samples of each of the powdered solids were compressed on the ATR crystal under a stainless-steel flat anvil with maximum load of 20 kg. For each liquid 1 mL was used without compression. All measurements were made at room temperature (23 °C).

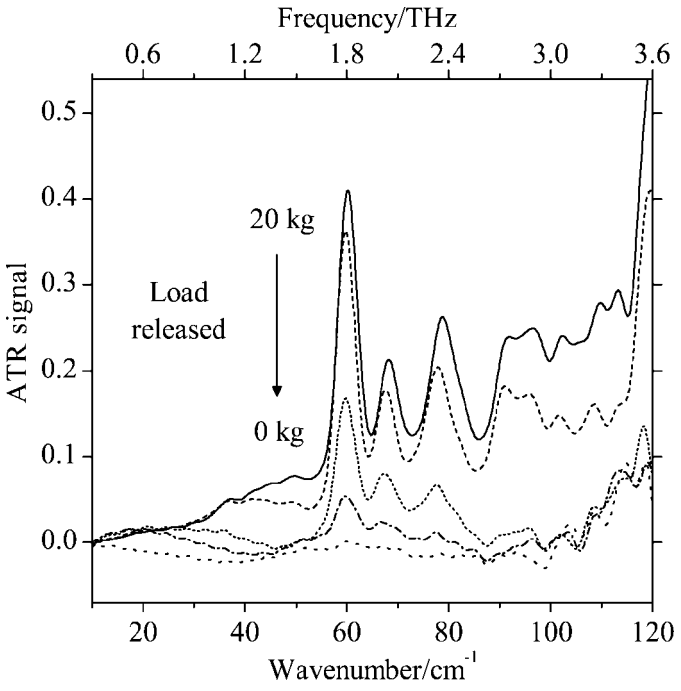

FIG. 4. Terahertz ATR spectra of L-ascorbic acid showing effect of releasing load.

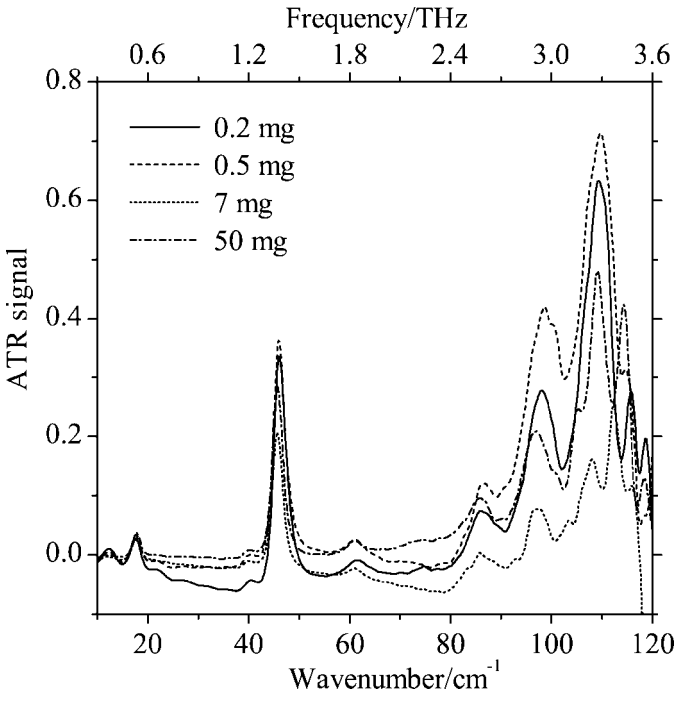

FIG. 5. Terahertz ATR spectra of α-lactose monohydrate showing effect of varying amount of sample.

RESULTS AND DISCUSSION

The measured terahertz ATR signal for L-ascorbic acid, an important anti-oxidant, is shown in Fig. 3. The ATR absorbance spectrum is calculated by automatically correcting for the frequency dependence of penetration depth. For comparison, a spectrum is shown for the corresponding transmission measurement of a 13 mm diameter pellet prepared

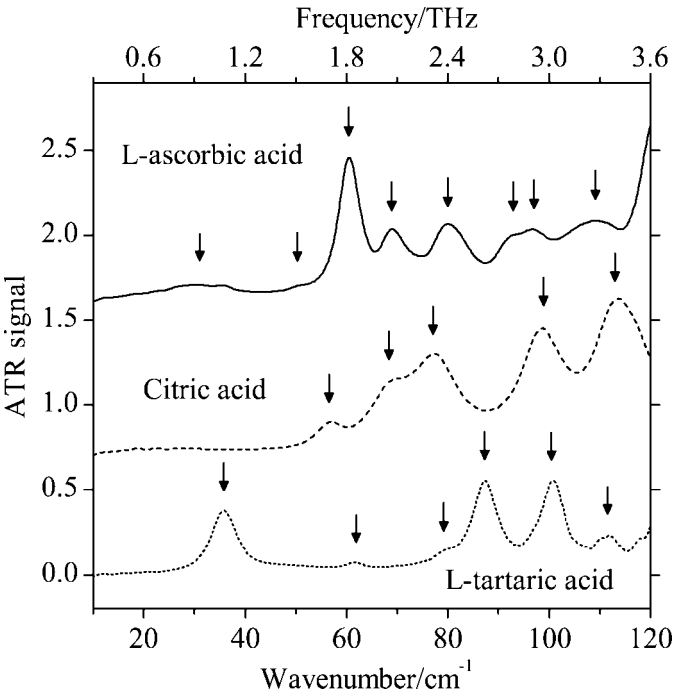

FIG. 6. Example terahertz ATR spectra of organic acids. Arrows indicate terahertz band positions (spectra offset for clarity.)

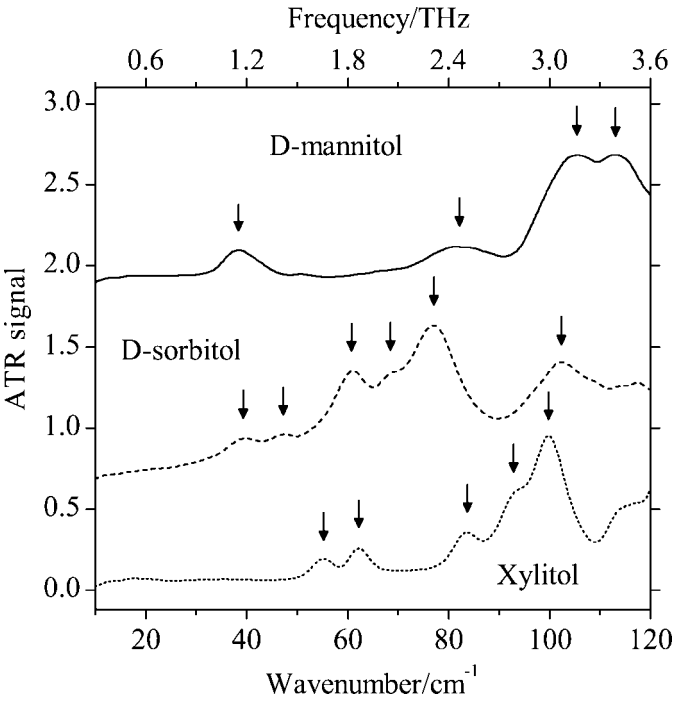

FIG. 7. Example terahertz ATR spectra of sugar alcohols. Arrows indicate terahertz band positions (spectra offset for clarity.)

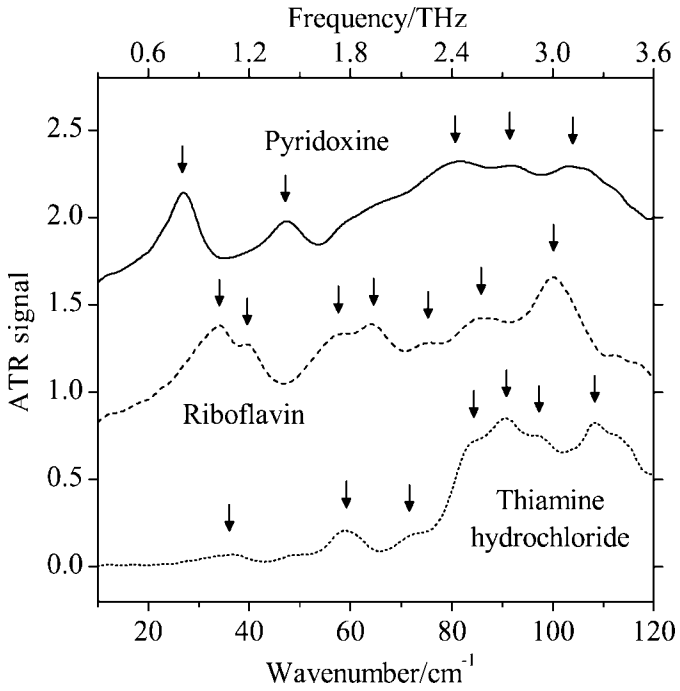

FIG. 8. Example terahertz ATR spectra of vitamins. Arrows indicate terahertz band positions (spectra offset for clarity.)

using 40 mg L-ascorbic acid physically mixed with 360 mg polyethylene powder and compressed. The transmission and ATR spectral signatures are similar although the transmission spectrum shows an underlying baseline that increases with wavenumber due to Mie scattering. In addition the attenuated reflection spectrum is slightly different from that in the absorption spectrum because of the large wavenumber of the evanescent wave.

The effect on terahertz spectra of L-ascorbic acid of releasing the ATR compression load is shown in Fig. 4. Absorbance decreases as contact between the sample and ATR crystal is lost, indicating that 20 kg load provides optimum sampling. This load, spread over the 7 mm diameter of the ATR crystal, is unlikely to induce pressure-induced changes in any but the most sensitive samples.

Figure 5 shows the ATR spectra of α-lactose monohydrate with different amounts placed onto the ATR crystal, showing that samples as small as 200 μg can be used.

Example terahertz ATR spectra of various solid materials are shown in Figs. 6–8. These materials have applications in the biotechnology, pharmaceutical, and food industries and have important biological functions, and some also find illicit uses. All of the materials show clear terahertz spectral signatures at room temperature with distinct absorption peaks in the 10 cm^{-1} to 120 cm^{-1} (0.3 THz to 3.6 THz) region. The positions of the principal absorption bands, arising from low-frequency vibrations and phonon modes in the hydrogen-bonded crystalline lattices, are listed in Table I. No band assignments are presented in this paper. Band assignments in the terahertz region is a complex and difficult subject but a number of groups around the world are beginning to develop the associated theory.[15–17]

Example terahertz ATR spectra of several liquids are shown in Fig. 9. Unlike the solid materials studied, these liquids show unstructured absorption due to the hydrogen-bonded networks and hindered molecular rotations.

CONCLUSION

Terahertz attenuated total reflection (ATR) spectra of solid materials and liquids covering the 10 cm^{-1} to 120 cm^{-1} (0.3

TABLE I. Principal terahertz ATR band positions for crystalline solid materials.

Material	Band positions /THz	Band positions /cm^{-1}
L-ascorbic acid (vitamin C)	1.08, 1.50, 1.80, 2.04, 2.34, 2.76, 2.91, 3.27	36, 50, 60, 68, 78, 92, 97, 109
Citric acid	1.71, 2.07, 2.31, 2.97, 3.42	57, 69, 77, 99, 114
L-tartaric acid	1.08, 1.86, 2.61, 3.03, 3.33	36, 62, 87, 101, 111
D-mannitol	1.14, 2.43, 3.18, 3.39	38, 81, 106, 113
D-sorbitol	1.20, 1.41, 1.83, 2.07, 2.31, 3.06	40, 47, 61, 69, 77, 102
Xylitol	1.65, 1.86, 2.52, 2.79, 3.00	55, 62, 84, 93, 100
Pyridoxine (vitamin B6)	0.81, 1.41, 2.46, 2.76, 3.09	27, 47, 82, 92, 103
Riboflavin (vitamin B2)	1.02, 1.17, 1.77, 1.92, 2.28, 2.58, 3.00	34, 39, 59, 64, 76, 86, 100
Thiamine hydrochloride (vitamin B1)	1.11, 1.77, 2.73, 2.91, 3.24	37, 59, 91, 97, 108

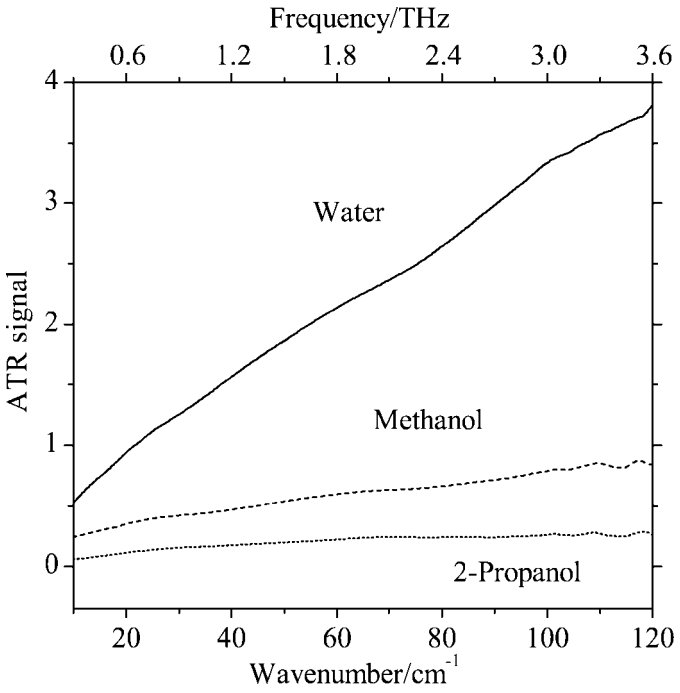

FIG. 9. Example terahertz ATR spectra of liquids (spectra not offset.)

THz to 3.6 THz) region are easily recorded using a terahertz pulsed spectrometer and silicon ATR modules. Terahertz ATR spectral signatures agree with those measured in transmission. With ATR only small amounts of sample—typically 1 mg for solids—are required, with no sample preparation, and the material can be recovered afterwards. Terahertz ATR allows the user to run many analyses in rapid sequence with no breaking of spectrometer purge, minimizing the interference of atmospheric water vapor absorption and the analysis time.

ACKNOWLEDGMENTS

The authors wish to thank the following people in the development of this work: Dr Julian Cluff for his excellent work on the optical design and Mr. John-Paul Cerroti for helpful discussions. The authors wish to acknowledge the valuable comments by the referees.

1. P. F. Taday, I. V. Bradley, D. D. Arnone, and M. Pepper, J. Pharm. Sci. **92,** 831 (2003).
2. C. J. Strachan, T. Rades, D. A. Newnham, K. C. Gordon, M. Pepper, and P. F. Taday, Chem. Phys. Lett. **390,** 20 (2004).
3. C. J. Strachan, P. F. Taday, D. A. Newnham, K. C. Gordon, J. A. Zeitler, M. Pepper, and T. Rades, J. Pharm. Sci. **94,** 837 (2005).
4. J. A. Zeitler, D. A. Newnham, P. F. Taday, T. L. Threlfall, R. W. Lancaster, R. W. Berg, C. J. Strachan, M. Pepper, K. C. Gordon, and T. Rades, J. Pharm. Sci. **95,** 2486 (2006).
5. J. A. Zeitler, K. Kogermann, J. Rantanen, T. Rades, P. F. Taday, M. Pepper, J. Aaltonen, and C. J. Strachan, Int. J. Pharm. **334,** 78 (2007).
6. H. B. Liu and X. C. Zhang, Chem. Phys. Lett. **429,** 229 (2006).
7. H.-B. Liu, Y. Chen, and X.-C. Zhang, J. Pharm. Sci. **96,** 927 (2007).
8. D. H. Auston, K. P. Cheung, and P. R. Smith, Appl. Phys. Lett. **45,** 284 (1984).
9. P. F. Taday and D. A. Newnham, Spectrosc. Eur. **16(5),** 20 (2004).
10. J. A. Zeitler, D. A. Newnham, P. F. Taday, C. J. Strachan, M. Pepper, K. C. Gordon, and T. Rades, Thermochim. Acta **436,** 71 (2005).
11. H. Hirori, K. Yamashita, M. Nagai, and K. Tanaka, Jpn. J. Appl. Phys. **43,** L1287 (2004).
12. M. Nagai, H. Yada, T. Arikawa, and K. Tanakas, Int. J. Infrared Millimeter Waves, **27,** 505 (2006).
13. N. J. Harrick, *Internal Reflection Spectroscopy* (John Wiley, New York, 1987), p. 43.
14. S. Ekgasit, Appl. Spectrosc. **54,** 756 (2000).
15. G. M. Day, J. A. Zeitler, W. Jones, T. Rades, and P. F. Taday, J. Phys. Chem., B **110,** 447 (2006).
16. D. G. Allis and T. M. Korter, Chem. Phys. Chem. **7,** 2398 (2006).
17. D. G. Allis, D. A. Prokhorova, and T. M. Korter, J. Phys. Chem. A **110,** 1951 (2006).